Diurnal changes of cyanobacteria blooms in Taihu Lake as derived from GOCI observations

Qi , L.; Hu, C.; Visser, P.M.; Ma, R.

DOI
10.1002/lno.10802

Publication date
2018

Document Version
Final published version

Published in
Limnology and Oceanography

LIMNOLOGY
and
OCEANOGRAPHY

ASLO

Limnol. Oceanogr. 63, 2018, 1711–1726

doi: 10.1002/lno.10802

Diurnal changes of cyanobacteria blooms in Taihu Lake as derived from GOCI observations

Lin Qi [1,2*] **Chuanmin Hu,** [3] **Petra M. Visser,** [4] **Ronghua Ma** [2*]

[1]State Key Laboratory of Marine Environmental Science, Xiamen University, Xiamen, China
[2]State Key Laboratory of Lake Science and Environment, Nanjing Institute of Geography and Limnology, Chinese Academy of Sciences, Nanjing, China
[3]College of Marine Science, University of South Florida, St. Petersburg, Florida, USA
[4]Department of Freshwater and Marine Ecology, Institute for Biodiversity and Ecosystem Dynamics, University of Amsterdam, Amsterdam, The Netherlands

Abstract

Using frequent and long-term measurements (eight times per day, 2011 to present) from a geostationary satellite sensor (Geostationary Ocean Color Imager, GOCI), this study investigates diurnal changes of cyanobacterium *Microcystis aeruginosa* blooms (near-surface high concentrations or surface scums) in Taihu Lake, from which vertical migration patterns could be inferred. After proper atmospheric correction, a cyanobacterial index algorithm is used to quantify equivalent surface cyanobacterial density (σ, 0–100%) at both pixel and synoptic scales from each cloud-free image, followed by analysis of diurnal changing patterns of σ at both scales. Three typical diurnal changing patterns are identified from all images, which show distinctive and different seasonality from the long-term statistics. Spatial distributions of the "hotspot" regions where diurnal changes are most often observed have also been established. While the seasonality of the three patterns appears to be a result of seasonality in both temperature and light availability, large blooms only occur 1 d after major wind events. Based on several lines of evidence, we hypothesize that the diurnal changes of such observed surface bloom patterns are likely a result of vertical migration rather than horizontal dissipation/aggregation of cyanobacteria. The mean migration speeds inferred from either a simple model or a radiative transfer model (< 0.03 cm s^{-1} or < 1 m h^{-1}) are consistent with those reported earlier from laboratory measurements for certain cyanobacteria colony sizes. Complete understanding of the three types of diurnal patterns and direct validation of the hypothesis, however, require further investigations from field measurements.

Cyanobacteria are ubiquitous phytoplankton often found in freshwaters, which can produce toxins to negatively impact ecosystem and human health (Gorham et al. 1964; Ganf 1974; Reynolds and Walsby 1975; Reynolds 1987; Paerl and Huisman 2008, 2009). Most freshwater cyanobacteria contain gas vesicles inside the cells (Bowen and Jensen 1965) (Fig. 1A), for example, *Microcystis aeruginosa* found in Taihu Lake and many other lakes. These gas vesicles can modulate cyanobacterial cell buoyancy, thus helping vertical movement of the cells to better utilize light (Reynolds and Walsby 1975; Reynolds 1987; Walsby and Bleything 1988; Kromkamp and Walsby 1990; Ibelings et al. 1991; Visser et al. 1997; Medrano et al. 2016*a*) and result in the forming of near-surface high concentrations of cells and surface scums (Fig. 1B). During daytime, the cell density increases because of photosynthesis-produced carbohydrates, making cells sink (Fig. 1C); during the night, the carbohydrates are respired, making cells rise (Walsby 1994; Wallace and Hamilton 1999; Wallace et al. 2000) (Fig. 1D). In addition to this mechanism, recent studies also found other factors that can modulate the cell movement (Dervaux et al. 2015; Medrano et al. 2016*b*). Cyanobacteria often form colonies in natural waters, where each colony is about 20–500 μm in diameter (Yamamoto and Shiah 2010; Qin et al. 2016) and composed of hundreds to thousands of cells embedded in mucilage, and in high-concentration colonies gas bubbles are formed within the colonies (Reynolds 1987; Walsby 1994; Medrano et al. 2016*b*). These gas bubbles (Fig. 1A), different from the gas vesicles inside the cells, contain oxygen produced by photosynthesis (Dervaux et al. 2015; Medrano et al. 2016*b*).

*Correspondence: lin.qi@xmu.edu.cn or rhma@niglas.ac.cn

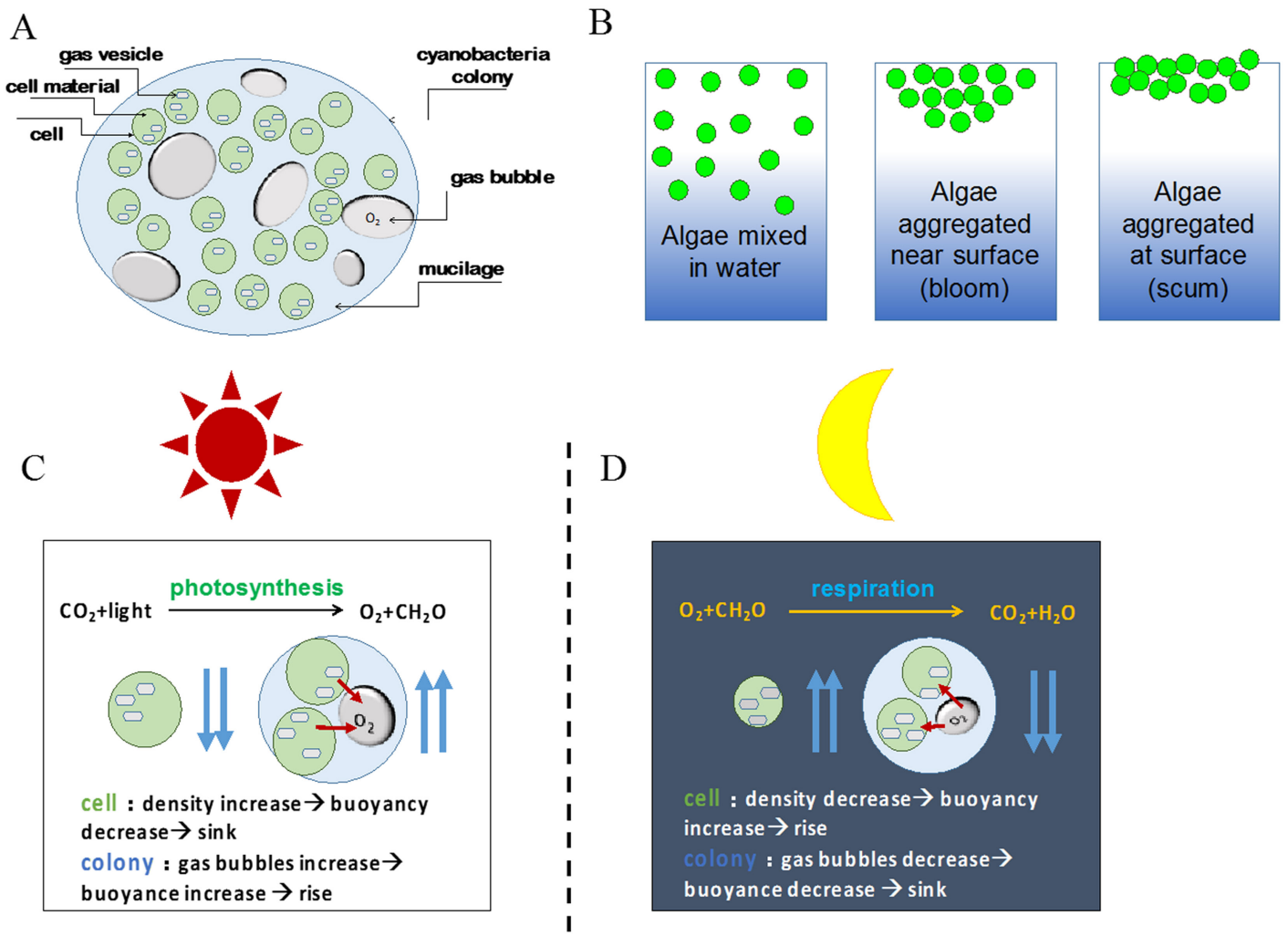

Fig. 1. (**A**) Illustration of gas vesicles inside cyanobacteria cells and gas bubbles between cyanobacteria cells within a cyanobacteria colony. Gas bubbles can form when colony concentrations are high; (**B**) illustration of cyanobacteria colonies mixed in water and cyanobacteria aggregated near surface and at surface (scum). In this study, the term "bloom" refers to the latter two cases. Here, "Algae" means cyanobacteria; (**C**, **D**) Illustration of vertical migration (both upward and downward) of cyanobacteria cells and colony during daytime (**C**) and nighttime (**D**).

These oxygen-containing gas bubbles can also modulate the colony movement as increased oxygen can facilitate the rise of colonies, and for the same reason decreased oxygen (through consumption by respiration or when bubbles break and escape from the colonies) can make the colonies sink. Therefore, vertical movement of cyanobacteria is modulated by changes in (1) cell density (through photosynthesis and respiration); (2) gas vesicles inside the cells; and (3) gas bubbles between cells in high-concentration colonies. In the real environment, temperature, light, wind, and hydrodynamics (e.g., turbulence) collectively modulate the vertical movement of cyanobacteria (Visser et al. 1995; Dervaux et al. 2015; Medrano et al. 2016*a*; Qin et al. 2016), through which surface scums may be formed and dissipated.

Nearly all observations of cyanobacterial vertical migration have been made from laboratory experiments under controlled conditions (Ganf 1974; Dervaux et al. 2015; Medrano et al. 2016*b*; Qin et al. 2016), as similar observations are difficult to make in natural environments (Ibelings et al. 1991). On the other hand, these observations are possible in the natural environments through satellite or airborne remote sensing. For example, Hunter et al. (2008) applied hyperspectral airborne measurements three times in a day over eutrophic waters of Barton Broad (United Kingdom) to study changes in pigment concentrations of cyanobacterium *M. aeruginosa*, which were interpreted as being caused by vertical movements of *Microcystis*. It has been difficult to extend the case study to other eutrophic lakes because hyperspectral airborne measurements are limited in both space and time. Satellite sensors provide synoptic and repeated measurements over the global aquatic environments, but lack of enough spectral bands and lack of accurate atmospheric

correction make it difficult to quantify pigment concentrations with sufficient accuracy to discern diurnal changes. Fortunately, *Microcystis* cells and colonies are known to be able to form scums or high-concentration near-surface layers due to vertical migration of cyanobacteria (Reynolds and Walsby 1975; Zohary and Robarts 1990) and such scums or near-surface blooms can be easily observed from satellite remote sensing without sophisticated algorithms. Indeed, their vertical migration may be observed indirectly from short-term (e.g., diurnal) changes of these surface blooms, where such changes can be quantified with measurements from the Geostationary Ocean Color Imager (GOCI, Ryu et al. 2012) that provides eight images a day. Indeed, observing cyanobacteria blooms (with cyanobacteria cells either mixed in the water column or aggregated near the surface) in lakes using satellite remote sensing is not new, but started decades ago. In this study, the term "bloom" specifically refers to the latter case where cyanobacteria cells form surface scums or aggregate near the surface through physical movement. In such cases, reflectance in the near-infrared (NIR) wavelengths is enhanced, and can appear similarly to those from land vegetation (i.e., red-edge reflectance) (Dekker et al. 2002), making it possible to quantify blooms. In other words, the term "bloom" in this study is defined in a practical sense where NIR reflectance in the 740–900 nm range is elevated due to surface scums or near-surface high cyanobacteria concentrations. This definition follows that of Reynolds and Walsby (1975) where changes in cyanobacteria buoyancy are the main drivers of the bloom formation, and this definition is different from the growth-based definition where the term "bloom" specifically refers phytoplankton biomass increases due to growth. Such a definition has also been used in other studies on short-term changes of cyanobacteria blooms in lakes (e.g., Wynne et al. 2010).

Given the known fact that cyanobacteria can migrate vertically through the water column during the course of a day and the potentials of frequent GOCI observations in quantifying short-term changes, the objectives of this study are:

1. Determine cyanobacteria equivalent surface density at both pixel and synoptic scales from GOCI imagery;
2. Quantify diurnal changes in cyanobacteria equivalent surface density and area, and document their typical diurnal changing patterns as well as potential "hotspots" of diurnal changes;
3. Estimate cyanobacteria vertical migration speed from the diurnal changing patterns, assuming these changes are due to vertical migration;
4. Analyze and discuss the environmental controls of the observed diurnal changes.

Taihu Lake is selected as the study region because it is a typical eutrophic lake with frequent cyanobacteria blooms (Kong et al. 2009; Hu et al. 2010) within the GOCI field of view. Furthermore, because of its location in the downstream of the Yangtze River and proximity to major cities and industry, cyanobacteria blooms are under influence of both climate variability and human activities, thus representing a good example for many other similar lakes in China and other countries. While numerous papers have been published on remote sensing of various water property parameters of Taihu Lake (Ma and Dai 2005; Wang et al. 2013; Qi et al. 2014; Huang et al. 2015; Shi et al. 2015), to date no study has documented long-term characteristics of diurnal changes of cyanobacteria surface density in this economically and environmentally important freshwater system.

Data and methods

GOCI and landsat-8 data processing

GOCI was launched in 2010 by the Korea Ocean Satellite Center (KOSC) of South Korea (Choi et al. 2012; Ryu et al. 2012). With a spatial resolution of 500 m, it has eight spectral bands centered at 412 nm, 443 nm, 490 nm, 555 nm, 660 nm, 680 nm, 745 nm, and 865 nm, respectively. Under typical top-of-atmosphere (TOA) radiance over the ocean, its signal-to-noise ratios (SNRs) in the visible bands are comparable to those of the Sea-viewing Wide Field-of-view Sensor (SeaWiFS) but in the NIR bands are much higher (about three times or 600 : 1) than those of SeaWiFS (Hu et al. 2012), making it more sensitive to detect subtle changes from the water signal. This is extremely important because the method used in this study to quantify cyanobacteria concentration mainly relies on the NIR bands, where the sensor's ability to detect partial bloom coverage within a pixel depends on the sensor's SNRs (Hu et al. 2015). With 1-h frequency, it measures the TOA radiance in the eight spectral bands eight times a day from $\sim$ 08:00 h to $\sim$ 15:00 h local time over a large region covering 2500 km $\times$ 2500 km centered at 36°N 130°E.

The Level-1 total radiance data have been transferred from KOSC to the U.S. NASA Goddard Space Flight Center in near real-time under an agreement. In this study, GOCI Level-1 data were downloaded from NASA GSFC (http://oceancolor.gsfc.nasa.gov) and processed to Level-2 data using the NASA software package SeaDAS (version 7.3). Because of the well-known difficulty in performing accurate atmospheric correction over turbid waters and surface cyanobacteria blooms, the processing only generated Rayleigh-corrected reflectance [$R_{rc}(\lambda)$, dimensionless, Eq. 1] for each image pixel, and the Level-2 R_{rc} data were subsequently mapped to a cylindrical-equidistant projection for further analysis (Hu et al. 2010).

For the period of 2011–2016, a total of 17,520 GOCI scenes were downloaded and processed to generate georeferenced $R_{rc}(\lambda)$ data. The $R_{rc}(\lambda)$ data in three spectral bands were used to compose false-color Red-Green-Blue (FRGB, R: 660 nm, G: 865 nm, B: 443 nm) images to visualize clouds and possible blooms. Each FRGB image was visually inspected, and images

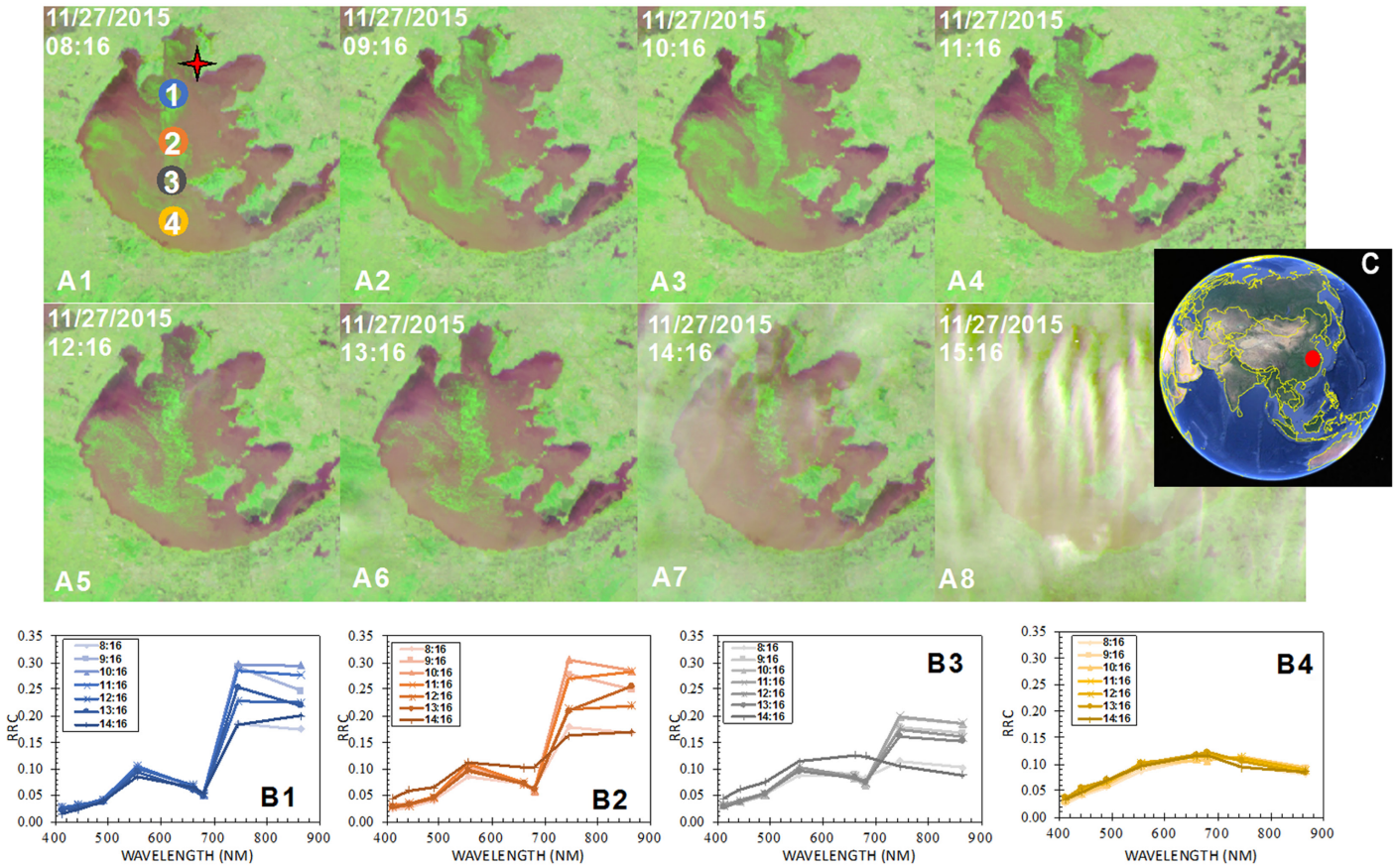

Fig. 2. (**A1**–**A8**) Eight GOCI FRGB images showing a daily sequence of cyanobacteria bloom (surface scums) in Taihu Lake [30.8°N to 31.6°N, 119.8°E to 120.8°E, location annotated on the Google-Earth map (**C**)] on 27 November 2015, where the location of wind speed measurement is annotated in (**A1**); (**B1**–**B4**) Diurnal changes of R_{rc} spectra from the four locations shown in (**A1**). A value of ~ 0.3 for R_{rc} in the NIR indicates that most of the GOCI pixel is covered by surface scum. Wind speed from a local meteorological station showed < 0.2 m s^{-1} between 08:00 h and 16:00 h.

with prevailing cloud cover were discarded. In total, 8000 relatively cloud-free GOCI scenes were used for subsequent analysis. Figure 2 top row shows a daily sequence of FRGB images on 27 November 2015, where R_{rc} spectra from four representative stations are presented in the bottom row.

Similar to GOCI processing, Landsat-8 Operational Land Imager (OLI) data were also processed to generate georeferenced R_{rc}, and then used to compose FRGB images using the corresponding OLI bands. These data were used to determine cyanobacteria-free water pixels and cyanobacteria-containing pixels in the corresponding GOCI imagery. Following the definition of bloom in this context (i.e., high near-surface concentrations or surface scums), "cyanobacteria-free" means that concentrations of cyanobacteria cells or colonies are not high enough near surface to cause a detectable NIR signal (see below).

Environmental data

Hourly wind velocity (V, m s^{-1}) and wind direction (W, °) were obtained from a Taihu Lake ecosystem field station located in the north of Taihu Lake (Fig. 2A1), which was maintained by the Chinese Academy of Sciences.

Surface temperature of Taihu Lake was estimated from MODIS sea surface temperature (SST, °C) data product. To avoid potential bias, only when $> 80\%$ of the lake was cloud free was temperature estimated as the average of the entire lake.

Surface instantaneous Photosynthetically Active Radiation (PAR) (iPAR, μmol photons m^{-2} s^{-1}) at any time of a day was calculated using the RADTRAN model (Gregg and Carder 1990). For a given location (in this case the location of the wind station) and time, solar zenith angle was first calculated. Then, assuming a coastal aerosol type and visibility of 10 km (corresponding to aerosol optical depth of about 0.2 at 860 nm, typical for Taihu Lake), surface iPAR was calculated through radiative transfer in the RADTRAN model.

Determine cyanobacteria equivalent areal density

Because of the enhanced reflectance in the NIR, bloom pixels in satellite imagery can be identified using the red and NIR wavelengths through several indexes such as band ratio (Duan et al. 2009), Normalized difference vegetation index (Zhou et al. 2008), and floating algae index (FAI, Hu 2009). Of these,

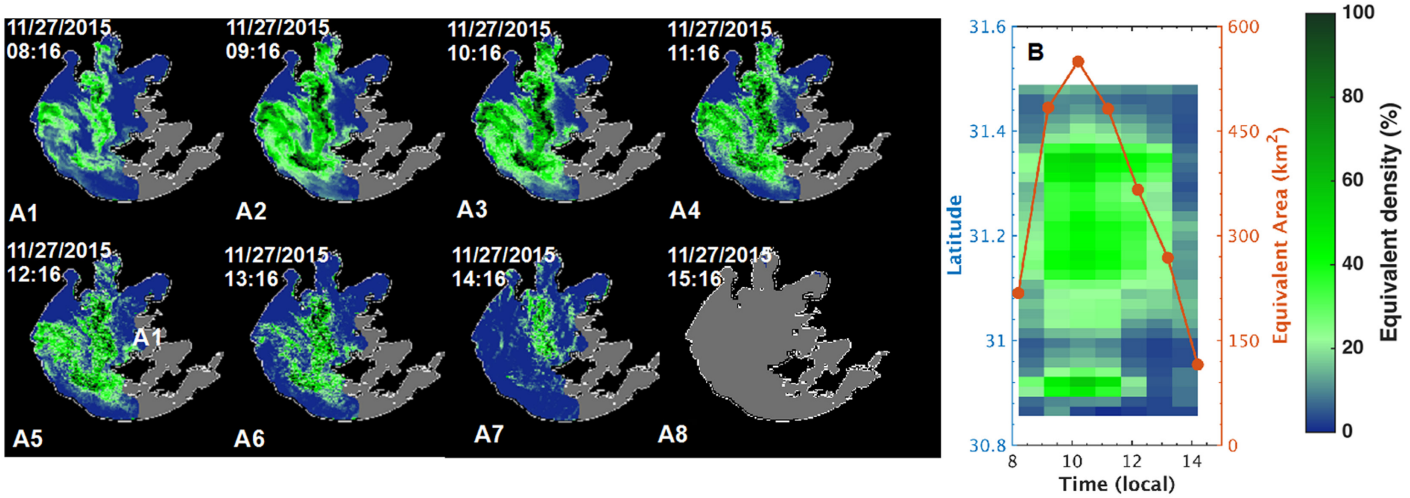

Fig. 3. Equivalent surface cyanobacteria density as a function of time (**A1**–**A8**), derived from GOCI measurements over Taihu Lake on 27 November 2015 (Fig. 2). The panel to the right in (**B**) shows the mean changes of cyanobacteria density as a function of time and latitude. Excluding the last hour, the total integrated surface cyanobacteria area varied between a minimum of 116 and a maximum of 550 km^2 (378 ± 163 km^2). Wind speed from a local meteorological station showed < 0.2 m s^{-1} between 08:00 h and 16:00 h.

FAI was found to be more tolerant than other indexes to changes in observing conditions (solar/viewing geometry, aerosols, etc.), thus more appropriate for quantitative analysis and time-series studies (Hu et al. 2010; Shang et al. 2011; Zhang et al. 2015). Therefore, following the concept of FAI used for MODIS to quantify cyanobacteria blooms in Taihu Lake (Hu et al. 2010), the lack of a shortwave infrared (SWIR) band on GOCI is remedied by an alternative FAI (AFAI) to replace the SWIR band with an NIR band:

$$\begin{aligned} &\mathrm{AFAI} = R_{\mathrm{rc},\lambda 2} - R_{\mathrm{rc},\lambda 2'} \\ &R_{\mathrm{rc},\lambda 2'} = R_{\mathrm{rc},\lambda 1} + (R_{\mathrm{rc},\lambda 3} - R_{\mathrm{rc},\lambda 1}) \times (\lambda_2 - \lambda_1)/(\lambda_3 - \lambda_1), \end{aligned} \quad (1)$$

Here, bands 1, 2, and 3 of GOCI are at 660 nm, 745 nm, and 865 nm, respectively. Figure 2 bottom row shows the R_{rc} spectra from eight GOCI measurements of the same pixels, where the changes in the NIR bands (and therefore the corresponding AFAI values) can be clearly seen.

Because of the linear subtraction design in AFAI, it is straightforward to determine the cyanobacteria areal density from linear unmixing of a pixel partially covered by the cyanobacteria bloom once two threshold values are defined. Following Qi et al. (2016) and Wang and Hu (2016), the two threshold values were first defined for the lower bound ($\mathrm{AFAI_L}$) and upper bound ($\mathrm{AFAL_H}$) of cyanobacteria-containing pixels. Below $\mathrm{AFAI_L}$, the pixel is regarded as a no-bloom pixel; above $\mathrm{AFAI_H}$, the pixel is regarded as having all (100%) cyanobacteria on the surface (i.e., 100% scum). An intermediate AFAI value indicates cyanobacteria approaching the surface from below, equivalent to a partial scum coverage within the pixel with the partial coverage determined through linear interpolation:

$$\alpha_i = (\mathrm{AFAI}_i - \mathrm{AFAI_L})/(\mathrm{AFAI_H} - \mathrm{AFAI_L}), \quad 0.0 < \alpha_i \le 1.0, \quad (2)$$

$\mathrm{AFAI_L}$ and $\mathrm{AFAI_H}$ were determined from concurrent GOCI and Landsat-8 OLI pairs through visual inspection of cyanobacteria-free GOCI pixels and cyanobacteria-containing GOCI pixels (100% coverage). Because of the resolution difference, each GOCI pixel (500-m) corresponds to ~ 278 OLI pixels (30-m), making it straight forward to determine whether a GOCI pixel is fully covered by cyanobacteria scum or not associated with bloom at all. In this study, they were determined to be −0.001 and 0.12, respectively. The AFAI value of 0.12 corresponds to the R_{rc} value of ~ 0.3 in the NIR, and such a high NIR reflectance in Taihu Lake has been confirmed to be associated with dense surface scum from field measurements. Figure 3 shows an example of diurnal changes of surface cyanobacteria density (α). Note that although for simplicity α is expressed as a % scum coverage within a pixel, in this study, it is an equivalent density (σ, 0–100%) whose change can also be a result of the vertical movement of cyanobacteria, with 100% representing cyanobacteria all aggregated on the very surface (i.e., scum) and < 100% representing high concentrations of cyanobacteria cells/colonies below the surface.

Quantify diurnal changes and vertical migration speed

Diurnal changes of equivalent surface cyanobacteria density were determined at both pixel level and synoptic scale in the lake. At these two scales, the cyanobacteria areal density (or integrated area) was plotted against time of the day, where diurnal changes of areal density were regarded as primarily a result of cyanobacteria vertical migration rather than horizontal aggregation/dissipation (*see* "Discussion"

section). Mean daily density change at a given pixel was first calculated as

$$\beta\left(\%\ \mathrm{h}^{-1}\right) = [1/(N-1)]\times\sum|(\alpha_{i+1}-\alpha_i)|, \quad i=0 \text{ to } N-1, \quad (3)$$

where N is number of total valid observations in a day ($N \leq 8$).

Then, two conceptual methods were used to estimate the vertical migration speed from the diurnal patterns.

The first was a simple estimate between the minimal and maximal density (or integrated area for large-scale changes), assuming that the cyanobacteria were concentrated in the middle of the water column and on the very surface of the water column, respectively:

$$V_1\left(\mathrm{m\ h}^{-1}\right) = 0.5\ Z_\mathrm{b}/(t_\mathrm{max}-t_\mathrm{min}), \quad (4)$$

where Z_b is the bottom depth, t_max and t_min correspond to the observing times of maximal and minimal density, respectively. The factor of 0.5 was to account for different vertical distributions of cyanobacteria, assuming that it is equivalent to have all cyanobacteria cells in the middle of the water column.

The second was based on a simplified radiative transfer model, where all hourly observations between t_min and t_max were used to fit the following equation:

$$\alpha(t) = \mathrm{C}_1(1-\exp(-2\ \mathrm{C}_2(t-t_0)) + \ \mathrm{C}_3 \quad (5)$$

where t is the GOCI time, α is the cyanobacteria density, t_0 is the time when cyanobacteria began to rise. C_1, C_2, and C_3 are numerical constants to be determined from nonlinear least-square fit between t and $\alpha(t)$. For the upward migration, when t approaches t_0, $\alpha(t)$ approaches the minimal density, C_3. When t approaches t_max, $\alpha(t)$ approaches the maximal density, $C_1 + C_3$. For the downward migration, similar interpretation can also be obtained. Here, C_2 represents the product of diffuse attenuation coefficient (K, m^{-1}) and vertical migration speed (V_2, m h^{-1}), and the factor of 2 was to account for the two-way attenuation. The functional form in Eq. 5 assumes that at $t = t_0$, all cyanobacteria were concentrated at an unknown depth, and this layer gradually moved to the surface, with its surface expression modulated by the two-way light attenuation.

Results

Diurnal patterns of surface cyanobacteria density

For all cloud-free days, diurnal changes of surface cyanobacteria density are observed clearly from the GOCI image series. Three typical patterns are observed, as shown in Fig. 4. The first pattern shows near-continuous increase over the course of a day (08:16 h to 15:16 h, local time) (Type 1, top row of Fig. 4), the second shows increasing density during the first few hours but decreasing density during the later hours (Type 2, second row of Fig. 4), and the third shows near-continuous decrease (Type 3, third row of Fig. 4). The total integrated equivalent surface cyanobacterial areas corresponding to these three types are shown in the bottom panels of Fig. 4.

Table 1 shows the statistics of the three types observed between 2011 and 2016. Only when at least six of the eight hourly measurements were cloud free were the observations used in calculating the statistics. Therefore, even though a total of 8000 relatively cloud-free hourly measurements were available, only a total of 106 cases with significant cyanobacteria blooms found in the imagery were used in the calculation. Of these, there is a clear difference between the seasonality of the three types. With a standard deviation of 39–61 d, Type 1 occurred around day 319, Type 2 occurred around day 277, and Type 3 occurred around day 222. There is also a clear difference between their maximal cyanobacteria coverage occurrence time, with Type 1 around 14:01 h, Type 2 around 11:42 h, and Type 3 around 08:48 h. Figure 5 also shows the seasonality of the daily maximum bloom occurrence time. In general, during summer, maximum cyanobacteria area was around 09:00 h, and the time moved to noon and early afternoon during the fall and early winter, respectively. On the other hand, nearly all these types occurred in the maximum bloom periods of July–October, as derived from phycocyanin concentration images (Qi et al. 2014).

"Hotspots" of diurnal changes

Figure 6 top row shows the spatial distributions of the equivalent surface cyanobacteria density (α in %, Eq. 2) and their seasonality, where the corresponding diurnal changes in the surface cyanobacteria density (β in % h^{-1}, Eq. 3) are presented in Fig. 6 bottom row. High cyanobacteria density occurred mainly in the NW of the lake during summer and fall, consistent with previous observations (Hu et al. 2010; Qi et al. 2014). These locations also represent the "hotspots" of diurnal changes, where hourly changes in surface cyanobacteria density can be a few percent for the entire season and could be much higher (a few 10 s of percent) for specific days.

Vertical migration speed

Using methods described above, V_1 (either upward or downward) from the hotspots of diurnal changes was estimated to be < 2 m per 2–4 h, or 0.028–0.014 cm s^{-1}. Migration speed V_2 was estimated through Eq. 5 as $\sim$ 0.3 m h^{-1} or 0.008 cm s^{-1} (assuming light attenuation, K, could be approximated by water absorption coefficient at 750 nm, $\sim$ 2.5 m^{-1}). These estimates are consistent with determinations from laboratory analyses of collected Taihu cyanobacteria samples (Qin et al. 2016) for the colony sizes of 64–100 μm (0.028 ± 0.008 cm s^{-1}) and 20–64 μm (0.008 ± 0.003 cm s^{-1}), respectively.

Response to wind

Wind plays an important role in affecting cyanobacteria vertical distributions. Under high winds the cells are well

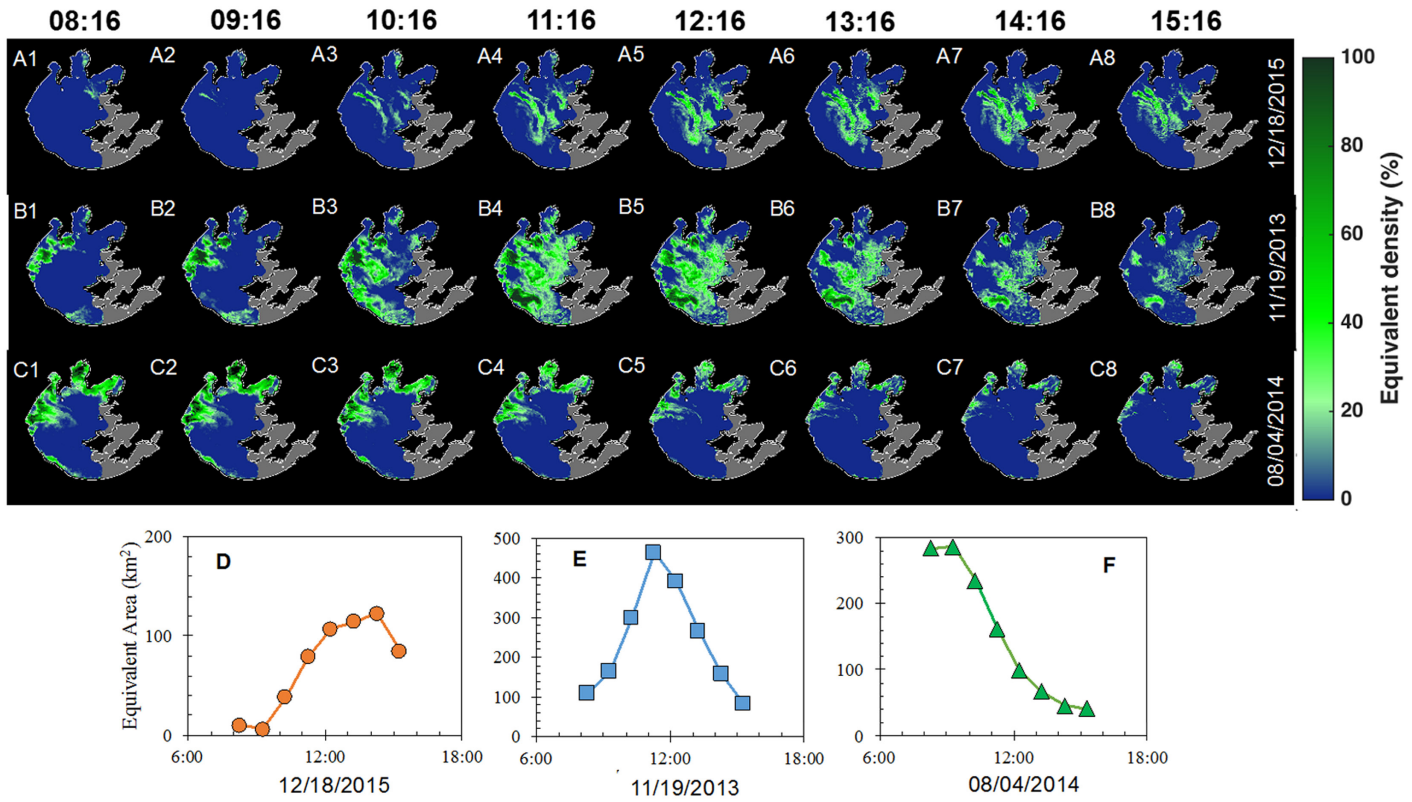

Fig. 4. Three typical types of diurnal change patterns of surface cyanobacteria density. Top row: Type 1—near-continuous increase (images collected on 18 December 2015, wind speed < 0.2 m s^{-1} between 08:00 h and 16:00 h); Second row: Type 2—increase first, and then decrease (images collected on 19 November 2013, wind speed < 2 m s^{-1} between 08:00 h and 16:00 h); Third row: Type 3—near-continuous decrease (images collected on 04 August 2014, wind speed < 2 m s^{-1} between 08:00 h and 16:00 h). Bottom panels in (**D**–**F**): Total integrated equivalent surface cyanobacteria areas corresponding to the three cases.

mixed in the water column, making it difficult to form scums or subsurface blooms. Such wind speed thresholds have been estimated through remote sensing observations to be around 3 m s^{-1} for Taihu Lake (Hu et al. 2010; Huang et al. 2015). The results from this study show two phenomena that have not been reported previously through remote sensing. The first is that only after major wind events did large blooms occur, and the second is that the blooms in the following days without new wind events became smaller.

Figure 7 and Table 2 show three groups of examples of such phenomenon. Group 1 (A1 and A2) shows that large blooms occurred 1 d after major wind events (mean speed > 4 m^{-1} during previous day); Group 2 (B1 and B2) shows that large blooms could also occur following the day when wind direction changed dramatically even though mean speed was < 3 m^{-1}; Group 3 (C1 and C2) shows that when mean speed was low (< 3 m^{-1}) and wind direction was also stable, blooms in the following day were relatively small. These observations are consistent with those based on field measurements but the GOCI-based study provides synoptic evidence. They are also consistent with those in Hunter et al. (2008) where high pigment concentrations were found immediately following high winds during the same day. Furthermore, Fig. 8 shows that major blooms occurred during only the first day after major wind events. During the second day after the wind event, even though wind remained continuously low, blooms were much smaller. Clearly, winds can not only change bloom patterns during the same day of wind observations (i.e., wind-induced mixing) but also affect bloom observations during subsequent days.

Discussion

Horizontal aggregation/dissipation or vertical migration?

Without *a priori* knowledge and in the absence of high winds, the change of a pixel's AFAI value during a day can be interpreted as from either (1) horizontal changes (i.e., dissipation or aggregation) or (2) vertical migration. Both can change the NIR signal and therefore AFAI value of the pixel. For the case of cyanobacteria blooms in Taihu Lake, the former is unlikely the cause for a number of reasons. First, decreases in cyanobacteria density of randomly selected GOCI pixels in one GOCI image were not accompanied by

Table 1. Statistics of the three typical types of diurnal change patterns of surface cyanobacterial area.

	Number of cases (2011–2016)	Proportion (%)	Max area (km^2)	Max area time (h)	Day of the year
Type 1	12	11	142.7 ± 47.2	14:01 ± 0.45	319 ± 39 (Oct–Dec)
Type 2	72	68	197.0 ± 111.4	11:42 ± 1.01	277 ± 56 (Aug–Nov)
Type 3	22	21	168.6 ± 94.5	08:48 ± 0.51	222 ± 61 (Jun–Oct)

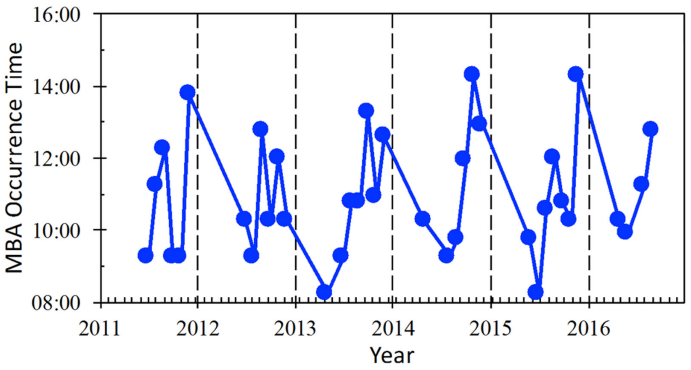

Fig. 5. MBA occurrence time (local time) in different days. The annotated year starts from January 1.

increases in spatially adjacent GOCI pixels in other images of the same day. From a simple mass balance, these changes could not be explained by horizontal redistribution of surface cyanobacteria. In other words, it is not logical to assume that from many adjacent pixels, each pixel has only a portion of cyanobacteria floating on the surface but the remaining portion has cyanobacteria all mixed in the water column. This may occur only on the boundary pixels of a large bloom patch but not in every pixel of the bloom. The same interpretation was used in Hunter et al. (2008) to explain temporal changes of pigment concentrations within 7 h from three repeated measurements over the same lake. Second, diurnal changing patterns of all three types often occurred in days with continuous low wind (sometimes more than 2 d), where vertical migration rather than horizontal aggregation or dissipation is likely the reason behind the changing patterns. Therefore, the only plausible explanation of the changing AFAI values over the course of a day in the absence of high-wind events is vertical migration of cyanobacteria. This is also why the surface density σ (Eq. 2) is interpreted as an equivalent density as some or most cells or colonies may be below the very surface to cause a partial coverage appearance.

Indeed, the definition of "bloom" in this study (surface scum or subsurface high concentrations of cyanobacteria that could lead to elevated NIR reflectance) is not based on biological growth but rather on physical aggregation. As stated by Reynolds and Walsby (1975), "bloom formation can occur when most of the algae possess excess buoyancy. Excess buoyancy is acquired when the photosynthetic rate is insufficient to develop the necessary turgor-pressure to cause collapse of the vacuoles." Following this definition, elevated NIR reflectance or AFAI signals do not necessarily require surface scums but can also result from near-surface high cyanobacteria concentrations. This has been demonstrated by Xue et al. (2015) through associating various vertical distribution types (Classes 1–4) and surface reflectance shapes. In Xue et al. (2015), both Classes 3 and 4 showed near-surface high concentrations of cyanobacteria, with the corresponding elevated NIR reflectance. Such elevated NIR reflectance not only occurred around 700–710 nm as shown in Gitelson (1992) and around 810 nm as shown in Kutser et al. (2016), but also occurred in wavelengths near the GOCI NIR bands of 745 nm and 865 nm to result in elevated AFAI values. Therefore, from a pure spectroscopy perspective, diurnal changes of surface density (derived from changes of AFAI values) can be interpreted as changes in cyanobacterial vertical distributions, as horizontal physical aggregation/dissipation are unlikely to explain such changes during perfectly calm days (Figs. 7, 8).

One may argue that although cross-pixel horizontal redistribution is unlikely the reason, intra-pixel redistribution could cause the observed diurnal changes because the coarse-resolution pixels may be mixed with bloom and non-bloom waters. This argument can be ruled out for two reasons. The first is that under perfectly calm days (Figs. 7, 8), it is difficult to understand why bloom patches within a 500-m pixel aggregate in the morning but dissipate in the afternoon. In contrast, respiration and photosynthesis appear to be more logical explanations if vertical movement is the reason behind the diurnal AFAI changes. Second, once the sensor has sufficient SNRs (i.e., sensitivity) in the NIR, even a small bloom patch within a pixel can be detected and expressed as a fractional bloom coverage (Eq. 2). For SNRs of 200 : 1, Hu et al. (2015) suggested that the smallest detectable patch is about 1–2% of a pixel size. For GOCI SNRs in the NIR of ~ 600 : 1 (Hu et al. 2012), the detection limit is about 0.3–0.7% of a pixel size. For elongated bloom patches (exceeding 500 m), the detection limit is about 2–3 m in width. The question then becomes whether most bloom patches in Taihu Lake are larger than 3 m × 500 m (or 1500 m^2, or near-surface bloom size has an equivalent surface expression > 1500 m^2). From comparison between near-simultaneous GOCI (500-m) and OLI (30-m) observations in Fig. 9, the answer appears to be yes. Although at pixel scale

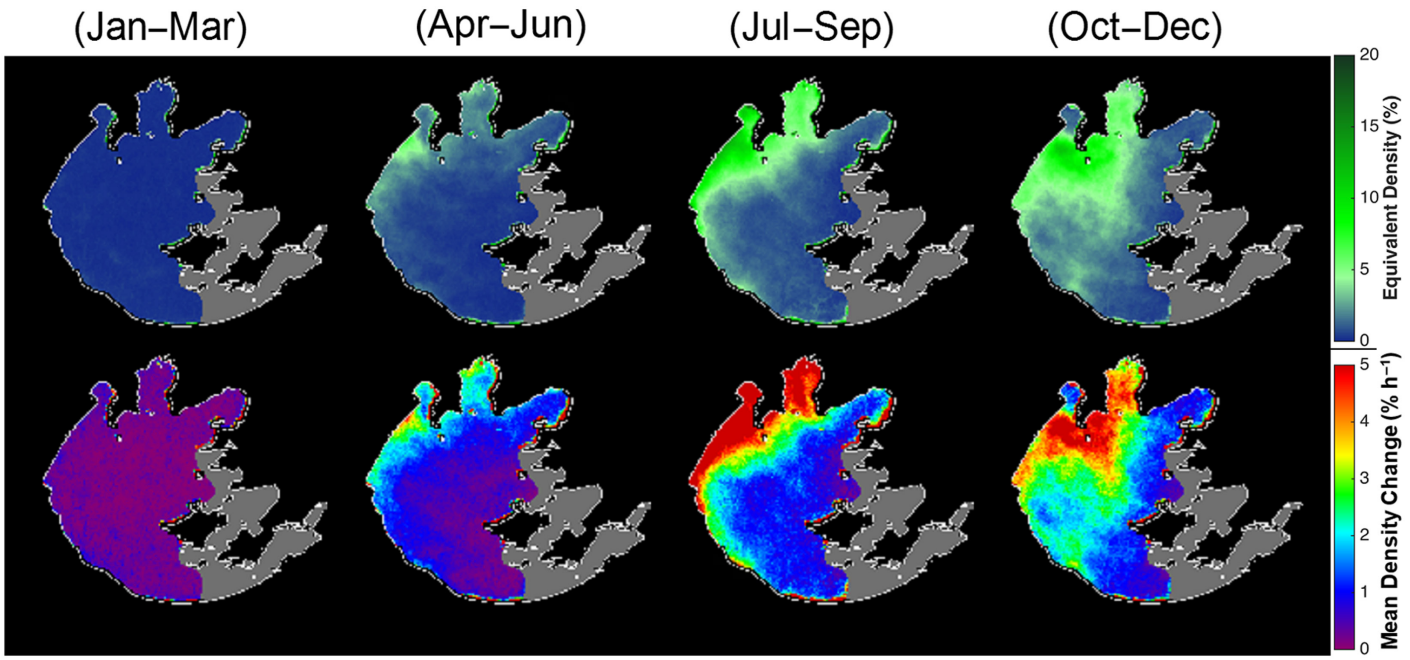

Fig. 6. Top: Seasonal variations of equivalent cyanobacteria density distributions (α in %, Eq. 2) between 2011 and 2017; Bottom: Seasonal variations of mean diurnal changes of surface cyanobacteria density (β in % h^{-1}, Eq. 3). The "hotspots" of diurnal changes (yellow and red colors) are found to correspond to high cyanobacteria density locations.

their fractional bloom coverage may be very different, at synoptic scale the spatial patterns of the fractional coverage are nearly identical. This is likely because that Taihu Lake is very shallow (mean water depth $\sim$ 2 m) and cyanobacteria concentrations can be much higher than in other regions such as the Baltic Sea. Kutser (2004) and Reinart and Kutser (2006) used 30-m resolution Hyperion to study cyanobacteria blooms in the Baltic Sea, and they argued that even the 30-m resolution sensor was not sufficient to capture scums. However, analysis of MODIS R_{rc} spectra from the 24 July 2002 image [the same image as used in Kutser (2004) and Reinart and Kutser (2006)] indicates that cyanobacteria blooms in the Baltic Sea are much less dense than in Taihu Lake, with R_{rc}(NIR) of rarely exceeding 0.03 (in contrast, R_{rc}(NIR) in Taihu Lake often exceeds 0.2 and can also reach 0.3; Fig. 2B). Therefore, GOCI 500-m resolution imagery with SNRs of $\sim$ 600 : 1 in the NIR appears to be sufficient to capture most bloom patches in Taihu Lake.

In short, although other possible processes leading to changes of algae density patterns cannot be completely ruled out due to lack of direct validation from field measurements, it is believed that vertical migration is the most logical explanation to interpret the observed diurnal changes in algae density patterns. Additional argument can also be found when environmental factors are used to explain the three different types of diurnal patterns, especially through photosynthesis-induced density increase (see below). There are numerous modeling studies (Visser et al. 1997; Wallace et al. 2000; Medrano et al. 2013, 2016*a*) and lab-based experiments (Ganf 1974; Medrano et al. 2013, 2016*b*) to document and explain the downward movement, and some limited field observations (e.g., Takamura and Yasuno 1984) also showed downward movement after forming a high-concentration near-surface layer. The spectral shapes and magnitudes bloom pixels in Fig. 2 indicate that although their NIR reflectance is high, in the visible domain their reflectance is still low, allowing light to penetrate the very surface to facilitate photosynthesis.

The migration speeds estimated here (0.008–0.028 cm s^{-1}), based on the hypothesis that diurnal changes of equivalent algae density are due to vertical migration rather than horizontal movement, are comparable to those determined from laboratory measurements (Qin et al. 2016) for colony size ranging between 24 μm and 100 μm but much lower than for larger sizes. This is possibly caused by turbulent conditions in the real environments, which were absent in the laboratory experiments. Although more sophisticated models have been developed to simulate cyanobacteria vertical migration under known light, wind, and turbulence conditions (Kromkamp and Walsby 1990; Visser et al. 1997), these models require more physiological model inputs than can be provided here. On the other hand, regardless of the modeling approach or parametrization, the simple estimate using Method 1 provides the upper bound of migration speed in a real environment: if it takes only 3 h to move all cyanobacteria from the 2-m bottom to the very surface, the

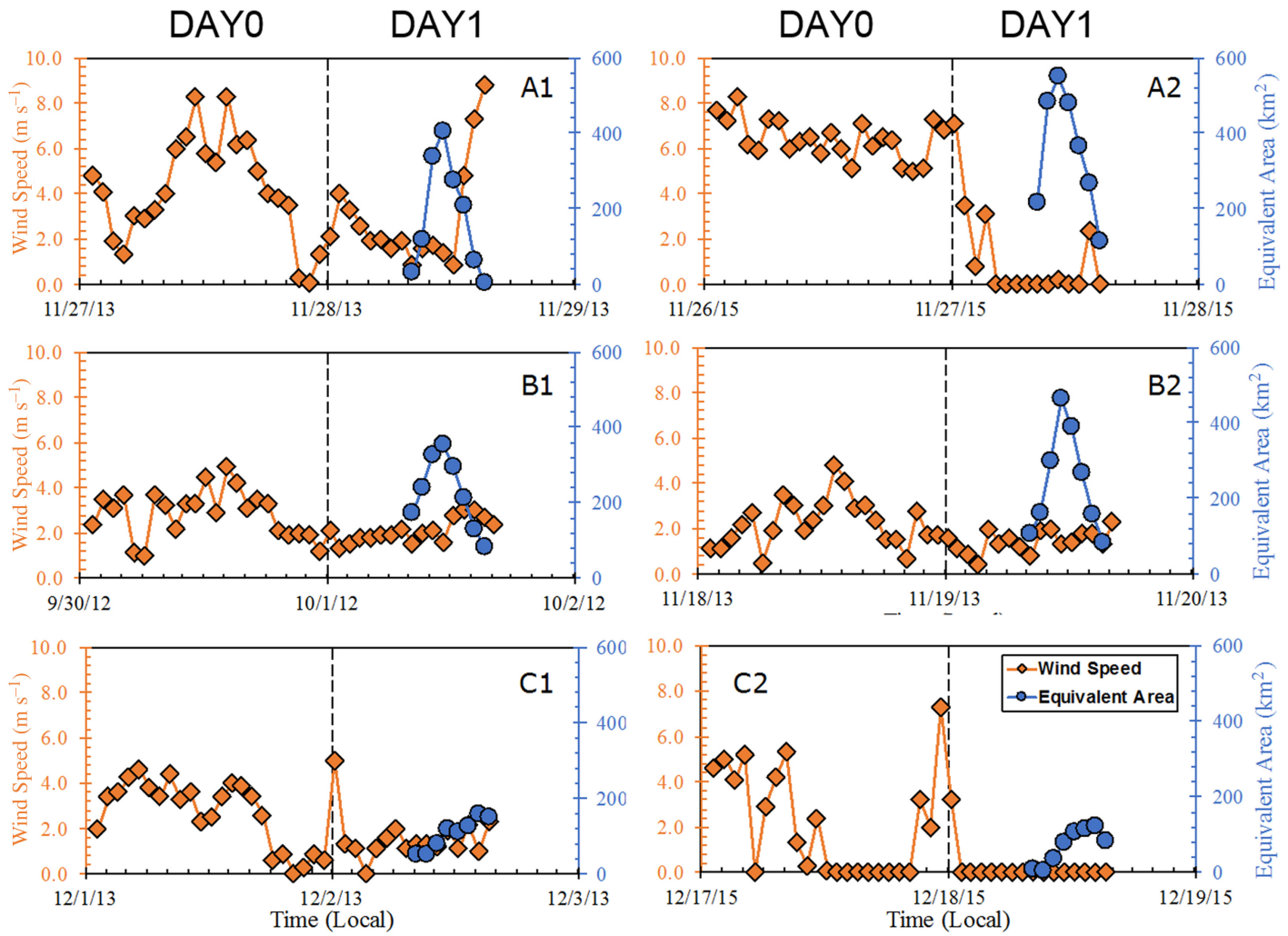

Fig. 7. Observations of blooms and winds for two consecutive days. Major blooms occurred immediately following major wind events. Statistics are presented in Table 2.

Table 2. Mean wind speed (*V*) and coefficient of variance (CV) of wind direction (*W*) before and during the major bloom days shown in Fig. 8. Note that the bloom area (BA) can be very large (bold font) when either wind speed or CV of wind direction of previous day is very high (bold font).

	Before bloom day (24 h)		During bloom day (08:00–15:00 h)		
Case ID	Mean of *V* (m s^{-1})	CV of *W*	Mean of *V* (m s^{-1})	CV of *W*	MBA (km^2)
A1	**4.1**	0.28	3.4	0.32	**406.7**
A2	**6.4**	0.02	0.3	0.24	**549.7**
B1	2.8	**0.87**	2.3	0.20	**353.0**
B2	2.2	**0.61**	1.5	0.44	**463.9**
C1	2.8	0.12	1.5	0.16	119.8
C2	2.1	0.29	0	—	123.2

MBA: maximum bloom area.

mean migration speed cannot exceed 0.7 m h^{-1}, still much lower than those reported from laboratory measurements for large colonies. On the other hand, this upper bound speed is in line with most observations of vertical migration of dinoflagellates, either in the lab or in the real environment (e.g., Hu et al. 2016).

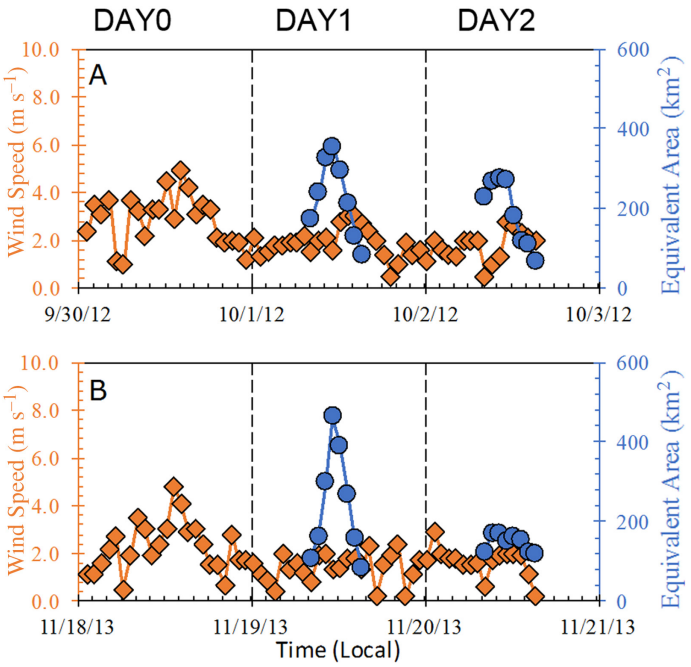

Fig. 8. Similar to Fig. 7, but blooms during the 2nd day (i.e., Day 2) after major wind events appeared to be smaller than during the 1st day (i.e., Day 1).

Finally, it is interesting to note that the three types of vertical migration patterns observed here are all different from those observed by Hunter et al. (2008) in the eutrophic lake of Barton Broad, where lowest concentrations were found around solar noon due to higher wind speed than in other times of the day.

Uncertainties in the estimates

Because all calculations were based on the diurnal GOCI AFAI changes, the first question is whether these changes are realistic or due to changes in the observing conditions (i.e., solar zenith angle, aerosols). The sensitivity of AFAI to solar zenith angle and aerosols was studied through the following equation

$$R_{rc,\lambda} = R_{t,\lambda} - R_{r,\lambda} = R_{a,\lambda} + t_\lambda \cdot t_{0,\lambda} \cdot R_{w,\lambda} \quad (6)$$

where $R_{t,\lambda}$ is the at-sensor total reflectance after adjusting for the two-way ozone absorption, $R_{a,\lambda}$ is reflectance due to scattering other than Rayleigh scattering (mostly aerosol scattering), $R_{w,\lambda}$ is the target reflectance. t_λ and $t_{0,\lambda}$ are the diffuse transmittance from the target to the satellite and from the sun to the target, respectively, which can be approximated as

$$t_\lambda \approx \exp(-0.5 \cdot \tau_{r,\lambda}/\cos\theta), \quad t_{0,\lambda} \approx \exp(-0.5 \cdot \tau_{r,\lambda}/\cos\theta_0) \quad (7)$$

Here $\tau_{r,\lambda}$ is the optical thickness of Rayleigh scattering (known from literature), θ is the sensor zenith angle (a constant because GOCI is geostationary, about 37° for Taihu), and θ_0 is the solar zenith angle that changes during the day.

The simulation calculated AFAI as a function of θ_0 under a given R_w and aerosol input, with results presented in Fig. 10. For the entire range of θ_0 during summer and winter, the change in AFAI is at most 5%. Similar results were obtained when aerosol optical thickness was changed. Therefore, for most cases, relative changes in AFAI due to changes in observing conditions are 5% or less, much lower than the observed diurnal changes from cyanobacteria or water pixels. Indeed, Fig. 2B4 shows very stable R_{rc} spectra over non-bloom waters for the entire day, and Fig. 2B1–B3 also show stable R_{rc} spectra over bloom waters for the visible wavelengths, both meaning that most R_{rc} changes in the red and NIR wavelengths (and therefore AFAI changes) are realistic rather than artifacts.

The simulations above assumed temporarily invariant R_w, but in reality R_w may change with θ_0 following the bloom's bidirectional reflectance distribution function (BRDF). Although BRDFs of many land surface types have been reported in the literature, BRDF of cyanobacteria blooms has not been reported. However, even if BRDF of cyanobacteria blooms could contribute to some of the observed diurnal bloom changes due to changes in solar zenith angle, such a contribution is unlikely to change with seasons, thus difficult to explain the three different types of diurnal change patterns in different times of a year.

Environmental controls of three types of diurnal changes

Under calm conditions (low wind velocity), vertical migration is mainly modulated by two processes: (1) upward movement due to gas vesicles inside cells and oxygen bubbles outside the cells but trapped within the colony mucus as well as decreased cell density due to respiration, and (2) downward movement due to increased cell density through photosynthesis and decreased oxygen bubbles (Fig. 1). The migration direction (upward or downward) is a result of these two competing processes. Then, why were three types of diurnal changes observed (Fig. 4; Table 1)?

The vertical migration pattern of Type III can be easily understood from density changes in the cells. The temperatures and light intensities (Fig. 11) are the highest when this type occurs (around Day 222, August) and consequently the density changes due to photosynthesis and respiration will be rapid. During the night, all colonies recover buoyancy and move to the surface where they become denser in the morning and start to sink when GOCI collects the first image of the day. Due to high iPAR and temperature, the photosynthesis rate is high enough that the downward movement overweighs the upward movement.

Type I shows an upward movement during the entire morning and early afternoon with a maximum surface density at 14:00 h. This type occurred around day 319 (Table 1) when

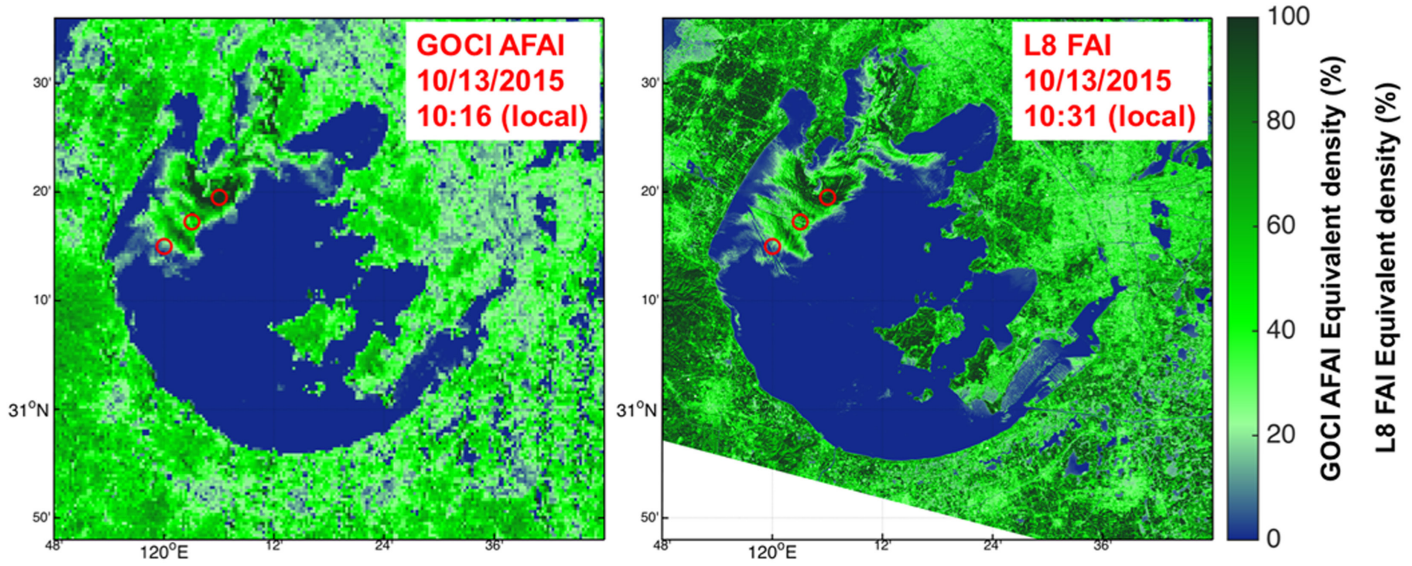

Fig. 9. GOCI AFAI (left) and L8 OLI FAI (right) images (after scaling to fractional bloom coverage within a pixel) on 13 October 2015 over Taihu Lake. The OLI image shows more details than the GOCI image that can be visualized after zoom-in, but the general patterns and magnitudes between the two images are nearly identical.

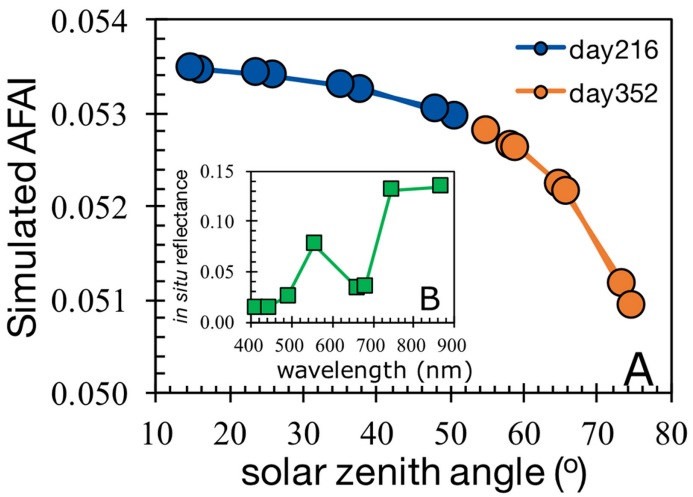

Fig. 10. (**A**) AFAI from a cyanobacteria pixel [R_w spectrum provided in (**B**), from Qi et al. 2014] as a function of solar zenith angle (i.e., time of day) for coastal aerosols (optical thickness at 860 nm = 0.15). Note the maximum change of only 5% for the entire sequence. [Color figure can be viewed at wileyonlinelibrary.com]

temperature is around 15°C (Fig. 11A). At these low temperatures, the rate of respiration is low (Visser et al. 1995) and recovery of buoyancy in the deeper, dark layers is a slow process. Consequently, the colonies only reach the surface slowly in the morning. For this type, photosynthesis is slow as iPAR is lower compared to the periods when the other two types occur, and thus the density increase is slow, causing delaying in the downward movement. The tipping point, when the downward movement overweighs the upward movement, is the latest in Type I compared to the other types. Actually Fig. 4A1–A8,D (Type 1) show that the last point at 14:16 h already shows a sign of downward migration. If GOCI measurements were to be extended further in later afternoon, for example, to 17:16 h, it is expected that such a downward migration would have continued.

Type II (∼ Day 277, October) is between Type 1 and Type III, where the tipping point occurred around solar noon. This type is more difficult to understand. The predominant upward movement in the morning is puzzling under the rather high iPAR and temperatures in this period. Type II occurs in periods (August–November) when the densities of cyanobacteria are relatively high. It might be explained by slightly lower temperatures and iPAR during this time of year compared to the Type III period, but if the pattern is compared with the modeled vertical migration patterns by Visser et al. (1997), this is only true for rather small colonies (< 100 μm). Since the majority of colonies is larger than 100 μm (Qin et al. 2016) in Taihu Lake, we suggest an alternative explanation. We hypothesize that the higher densities in this time of year (as can be seen in Fig. 4B) result in gas bubbles by late morning that are trapped in the mucus layer of the colonies (Dervaux et al. 2015; Medrano et al. 2016*b*). Consequently, accumulation of carbohydrates should be higher to counterbalance this positive buoyancy before the colonies can sink, and the cells will need more time to break down this higher carbohydrate content. This may explain the late arrival in the morning, which again depends on the colony size.

To evaluate whether these hypotheses for the migration types are valid, density changes of colonies from Taihu Lake

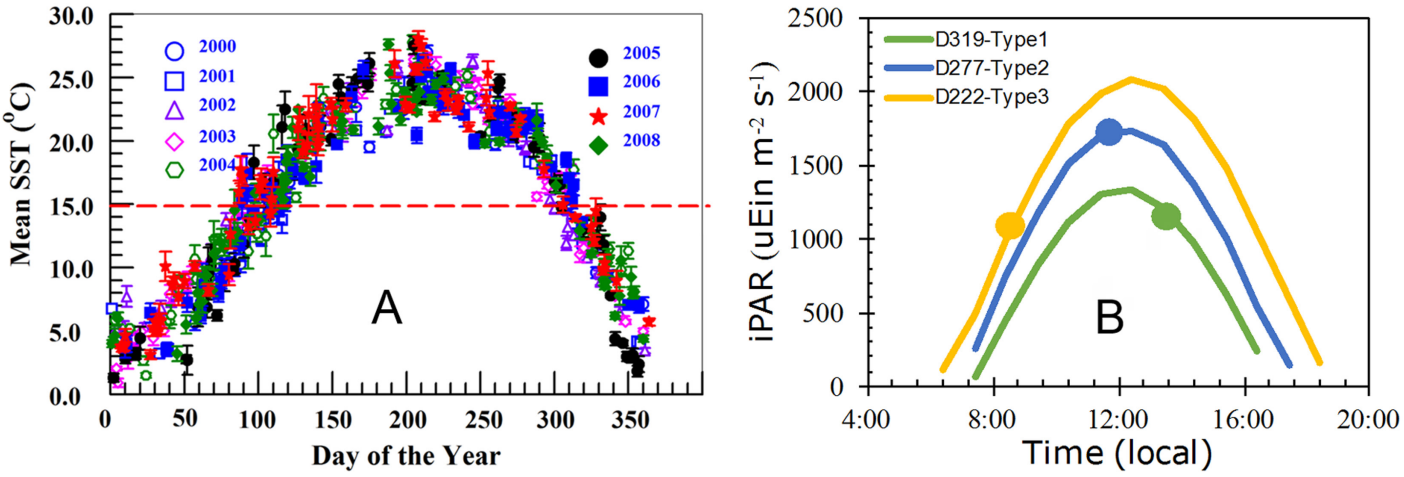

Fig. 11. (**A**) MODIS mean daily SST over the entire Taihu Lake during cloud-free days of 2000–2008. Annotated is a dashed line denoting 15°C (below 15°C respiration is lower than photosynthesis resulting in accumulation of carbohydrates, Visser et al. 1995), corresponding to about day 100 (10 April) and 310 (06 November), respectively; (**B**) Surface iPAR as a function of time for Days 319 (Type 1), 277 (Type 2), and 222 (Type 3). The mean local time of a day corresponding to MBA for each of the three types is annotated with a solid circle.

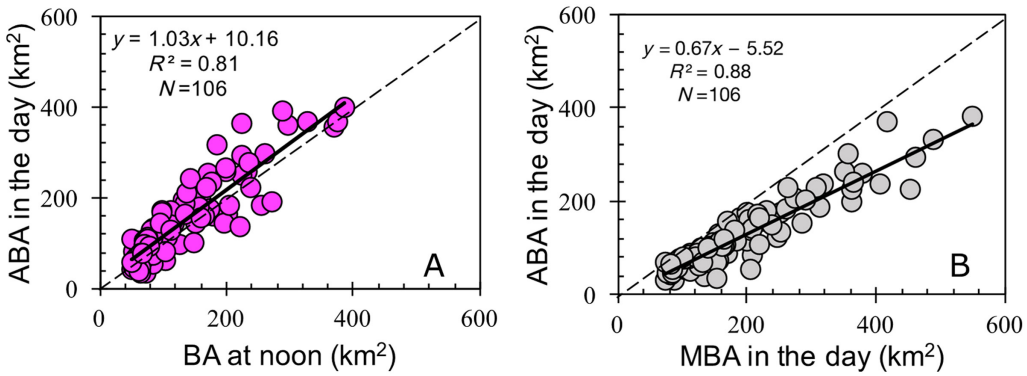

Fig. 12. (**A**) bloom area (BA) at 12:16 h vs. average bloom area (ABA) of the day; (**B**) MBA vs. ABA of the day.

could be investigated in relation to light intensity and temperature and incorporated in a model (e.g., Visser et al. 1997) to describe the vertical migration of colonies in Taihu Lake at different times of the year. Additionally, other physical factors such as turbulence may also be incorporated in the model, although it is speculated that turbulence is unlikely to change the seasonality of the diurnal patterns under similar wind conditions. Furthermore, because river input is mostly restricted to nearshore waters, river input might not be a major factor either. In any case, direct field measurement is required to validate the hypotheses, for example, through continuous measurements of cyanobacteria fluorescence or scattering at multiple depths using moored sensors.

Implications on bloom dynamics and bloom monitoring

Because many phytoplankton (e.g., dinoflagellates) can also move vertically in various marine and freshwater systems (Kamykowski et al. 1992; Schofield et al. 2006; Schaeffer et al. 2009), this research represents one of the pilot efforts and may also serve as a template toward future remote sensing studies of phytoplankton dynamics and their response to environmental changes in natural environments. For example, using GOCI images, Lou and Hu (2014) showed changes in bloom size of the dinoflagellate *Prorocentrum donghaiense* in the East China Sea, and such changes were speculated to be a result of dinoflagellate vertical movement. Likewise, Qi et al. (2017) used Visible Infrared Imaging Radiometer Suite (VIIRS) imagery to show intra-day changes of blooms of the dinoflagellate *Karenia brevis*, which were confirmed by glider measurements to be a result of *K. brevis* vertical migration. These previous studies, however, only provided bloom patterns of algae mixed in the water column. The current study is focused on surface scums or near-surface blooms of cyanobacteria, which are subject to lower uncertainties and easier to interpret under

calm conditions. The method might be extendable to studies of dinoflagellates when they also form surface scums or near surface blooms.

While GOCI provides unique observations of diurnal changes of bloom patterns, such a capacity is not available from other satellite sensors that have often been used by the community to monitor bloom changes in near real-time and bloom trends in the long run (e.g., Hu et al. 2010). The question then arises whether the polar-orbiting satellites, which can provide at most one observation a day (usually around solar noon) for subtropical and tropical waters, can lead to reliable estimates of long-term bloom patterns. Figure 12 shows a comparison between the various observing schemes. In Fig. 12A, bloom areas (BAs) from snapshot GOCI observations around solar noon are compared with the mean daily BAs (6–8 cloud-free measurements). Overall, they are comparable, with the fitting line close to the 1 : 1 line. However, there is also a large data spread around the 1 : 1 line, indicating that if the number of cloud free days is not large enough the uncertainties in the mean monthly BAs could be very high. Likewise, in Fig. 12B, if a daily maximum bloom area (MBA) were used to represent the daily mean BA, an overestimate would result. Clearly, more observations from GOCI would reduce uncertainties in deriving the "mean" bloom conditions, thus providing more reliable estimates in long-term bloom patterns.

Conclusion

Using frequent GOCI observations, typical types of diurnal changing patterns in cyanobacteria blooms (surface scums or near-surface high concentrations) of Taihu Lake are determined. These patterns show clear seasonality that can be explained conceptually using temperature, light availability, and photosynthesis. Wind also plays a significant role as major blooms are only found after major wind events. Most importantly, from several lines of evidence, it is hypothesized that the diurnal bloom patterns could primarily be caused by vertical migration of cyanobacteria cells and/or colonies, whose migration speeds are estimated to be in line with those determined from laboratory experiments for certain colony sizes. While direct field measurements are still required to test the hypothesis, the study shows unique values of geostationary sensors in their capacity to study short-term phytoplankton dynamics in the real environments, which not only helps to understand phytoplankton dynamics at synoptic scales but also provides guidance for future targeted sampling to the hotspots of diurnal changes.

References

Bowen, C., and T. Jensen. 1965. Blue-green algae: Fine structure of the gas vacuoles. Science **147**: 1460–1462. doi:10.1126/science.147.3664.1460

Choi, J.-K., Y. J. Park, J. H. Ahn, H.-S. Lim, J. Eom, and J.-H. Ryu. 2012. GOCI, the world's first geostationary ocean color observation satellite, for the monitoring of temporal variability in coastal water turbidity. J. Geophys. Res. Oceans **117**: 2156–2202. doi:10.1029/2012JC008046

Dekker, A. G., and others. 2002. Imaging spectrometry of water, p. 307–359. *In* F. D. van der Meer and S. M. de Jong [eds.], Imaging spectrometry: Basic principles and prospective applications. Netherlands: Kluwer Academic Publishers.

Dervaux, J., A. Mejean, and P. Brunet. 2015. Irreversible collective migration of cyanobacteria in eutrophic conditions. PLoS One **10**: e0120906. doi:10.1371/journal.pone.0120906

Duan, H., R. Ma, X. Xu, F. Kong, S. Zhang, W. Kong, J. Hao, and L. Shang. 2009. Two-decade reconstruction of algal blooms in China's Lake Taihu. Environ. Sci. Technol. **43**: 3522–3528. doi:10.1021/es8031852

Ganf, G. 1974. Diurnal mixing and the vertical distribution of phytoplankton in a shallow equatorial lake (Lake George, Uganda). J. Ecol. **62**: 611–629. doi:10.2307/2259002

Gitelson, A. A. 1992. The peak near 700 nm on radiance spectra of algae and water: Relationships of its magnitude and position with chlorophyll concentration. Int. J. Remote Sens. **13**: 3367–3373. doi:10.1080/01431169208904125

Gorham, P., J. McLachlan, U. Hammer, and W. Kim. 1964. Isolation and culture of toxic strains of Anabaena flos-aquae (Lyngb.) de Breb. Verh. Int. Ver. Theor. Angew. Limnol. **15**: 796–804. doi:10.1080/03680770.1962.11895606

Gregg, W. W., and K. L. Carder. 1990. A simple spectral solar irradiance model for cloudless maritime atmospheres. Limnol. Oceanogr. **35**: 1657–1675. doi:10.4319/lo.1990.35.8.1657

Hu, C. 2009. A novel ocean color index to detect floating algae in the global oceans. Remote Sens. Environ. **113**: 2118–2129. doi:10.1016/j.rse.2009.05.012

Hu, C., Z. Lee, R. Ma, K. Yu, D. Li, and S. Shang. 2010. Moderate resolution imaging spectroradiometer (MODIS) observations of cyanobacteria blooms in Taihu Lake, China. J. Geophys. Res. Oceans **115**: C04002. doi:10.1029/2009JC005511

Hu, C., L. Feng, and Z. Lee. 2012. Evaluation of GOCI sensitivity for at-sensor radiance and GDPS-retrieved chlorophyll-a products. Ocean Sci. J. **47**: 279–285. doi:10.1007/s12601-012-0028-0

Hu, C., L. Feng, R. F. Hardy, and E. J. Hochberg. 2015. Spectral and spatial requirements of remote measurements of pelagic *Sargassum* macroalgae. Remote Sens. Environ. **167**: 229–246. doi:10.1016/j.rse.2015.05.022

Hu, C., B. B. Barnes, L. Qi, C. Lembke, and D. English. 2016. Vertical migration of *Karenia brevis* in the northeastern Gulf of Mexico observed from glider measurements. Harmful Algae **58**: 59–65. doi:10.1016/j.hal.2016.07.005

Huang, C., and others. 2015. Satellite observation of hourly dynamic characteristics of algae with Geostationary Ocean Color Imager (GOCI) data in Lake Taihu. Remote Sens. Environ. **159**: 278–287. doi:10.1016/j.rse.2014.12.016

Hunter, P. D., A. N. Tyler, N. J. Wilby, and D. J. Gilvear. 2008. The spatial dynamics of vertical migration by *Microcystis aeruginosa* in a eutrophic shallow lake: A case study using high spatial resolution time-series airborne remote sensing. Limnol. Oceanogr. **53**: 2391–2406. doi:10.4319/lo.2008.53.6.2391

Ibelings, B. W., L. R. Mur, and A. E. Walsby. 1991. Diurnal changes in buoyancy and vertical distribution in populations of *Microcystisin* two shallow lakes. J. Plankton Res. **13**: 419–436. doi:10.1093/plankt/13.2.419

Kamykowski, D., R. E. Reed, and G. J. Kirkpatrick. 1992. Comparison of sinking velocity, swimming velocity, rotation and path characteristics among six marine dinoflagellate species. Mar. Biol. **113**: 319–328. doi:10.1007/BF00347287

Kong, F. X., R. Ma, J. Gao, and X. Wu. 2009. The theory and practice of prevention, forecast and warning on cyanobacteria bloom in Lake Taihu [in Chinese]. J. Lake Sci. **21**: 314–328. doi:10.18307/2009.0302

Kromkamp, J., and A. E. Walsby. 1990. A computer model of buoyancy and vertical migration in cyanobacteria. J. Plankton Res. **12**: 161–183. doi:10.1093/plankt/12.1.161

Kutser, T. 2004. Quantitative detection of chlorophyll in cyanobacterial blooms by satellite remote sensing. Limnol. Oceanogr. **49**: 2179–2189. doi:10.4319/lo.2004.49.6.2179

Kutser, T., B. Paavel, C. Verpoorter, M. Ligi, T. Soomets, K. Toming, and G. Casal. 2016. Remote sensing of black lakes and using 810 nm reflectance peak for retrieving water quality parameters of optically complex waters. Remote Sens. **8**: 497. doi:10.3390/rs8060497

Lou, X., and C. Hu. 2014. Diurnal changes of a harmful algal bloom in the East China Sea: Observations from GOCI. Remote Sens. Environ. **140**: 562–572. doi:10.1016/j.rse.2013.09.031

Ma, R., and J. Dai. 2005. Investigation of chlorophyll-a and total suspended matter concentrations using Landsat ETM and field spectral measurement in Taihu Lake, China. Int. J. Remote Sens. **26**: 2779–2795. doi:10.1080/01431160512331326648

Medrano, E. A., R. Uittenbogaard, L. D. Pires, B. Van De Wiel, and H. Clercx. 2013. Coupling hydrodynamics and buoyancy regulation in *Microcystis aeruginosa* for its vertical distribution in lakes. Ecol. Model. **248**: 41–56. doi:10.1016/j.ecolmodel.2012.08.029

Medrano, E. A., B.J.H.V. De Wiel, R. E. Uittenbogaard, L. M. D. Pires, and H. J. H. Clercx. 2016*a*. Simulations of the diurnal migration of *Microcystis aeruginosa* based on a scaling model for physical-biological interactions. Ecol. Model. **337**: 200–210. doi:10.1016/j.ecolmodel.2016.06.019

Medrano, E. A., R. E. Uittenbogaard, B.J.H.V. De Wiel, L. M. D. Pires, and H. J. H. Clercx. 2016*b*. An alternative explanation for cyanobacterial scum formation and persistence by oxygenic photosynthesis. Harmful Algae **60**: 27–35. doi:10.1016/j.hal.2016.10.002

Paerl, H. W., and J. Huisman. 2008. Blooms like it hot. Science **320**: 57–58. doi:10.1126/science.1155398

Paerl, H. W., and J. Huisman. 2009. Climate change: A catalyst for global expansion of harmful cyanobacterial blooms. Environ. Microbiol. Rep. **1**: 27–37. doi:10.1111/j.1758-2229.2008.00004.x

Qi, L., C. Hu, H. Duan, J. Cannizzaro, and R. Ma. 2014. A novel MERIS algorithm to derive cyanobacterial phycocyanin pigment concentrations in a eutrophic lake: Theoretical basis and practical considerations. Remote Sens. Environ. **154**: 298–317. doi:10.1016/j.rse.2014.08.026

Qi, L., C. Hu, Q. Xing, and S. Shang. 2016. Long-term trend of *Ulva prolifera* blooms in the western Yellow Sea. Harmful Algae **58**: 35–44. doi:10.1016/j.hal.2016.07.004

Qi, L., C. Hu, B. B. Barnes, and Z. Lee. 2017. VIIRS captures phytoplankton vertical migration in the NE Gulf of Mexico. Harmful Algae **66**: 40–46. doi:10.1016/j.hal.2017.04.012

Qin, B., and others. 2016. Dynamics of variability and mechanism of harmful cyanobacteria bloom in Lake Taihu, China [in Chinese]. Chin. Sci. Bull. **61**: 759–770. doi:10.1360/N972015-00400

Reinart, A., and T. Kutser. 2006. Comparison of different satellite sensors in detecting cyanobacterial bloom events in the Baltic Sea. Remote Sens. Environ. **102**: 74–85. doi:10.1016/j.rse.2006.02.013

Reynolds, C. S. 1987. Cyanobacterial water-blooms. Adv. Bot. Res. **13**: 67–143. doi:10.1016/S0065-2296(08)60341-9

Reynolds, C. S., and A. E. Walsby. 1975. Water-blooms. Biol. Rev. **50**: 437–481. doi:10.1111/j.1469-185X.1975.tb01060.x

Ryu, J.-H., H.-J. Han, S. Cho, Y.-J. Park, and Y.-H. Ahn. 2012. Overview of geostationary ocean color imager (GOCI) and GOCI data processing system (GDPS). Ocean Sci. J. **47**: 223–233. doi:10.1007/s12601-012-0024-4

Schaeffer, B. A., D. Kamykowski, G. Sinclair, L. McKay, and E. J. Milligan. 2009. Diel vertical migration thresholds of *Karenia brevis* (Dinophyceae). Harmful Algae **8**: 692–698. doi:10.1016/j.hal.2009.01.002

Schofield, O., J. Kerfoot, K. Mahoney, M. Moline, M. Oliver, S. Lohrenz, and G. Kirkpatrick. 2006. Vertical migration of the toxic dinoflagellate *Karenia brevis* and the impact on ocean optical properties. J. Geophys. Res. **111**: C06009. doi:10.1029/2005JC003115

Shang, L., R. Ma, H. Duan, G. Jiang, and L. Zhou. 2011. Scale analysis of cyanobacteria bloom in Lake Taihu from MODIS observations [in Chinese]. J. Lake Sci. **23**: 847–854. doi:10.18307/2011.0604

Shi, K., and others. 2015. Long-term remote monitoring of total suspended matter concentration in Lake Taihu using 250m MODIS-Aqua data. Remote Sens. Environ. **164**: 43–56. doi:10.1016/j.rse.2015.02.029

Takamura, N., and M. Yasuno. 1984. Diurnal changes in the vertical distribution of phytoplankton in hypertrophic Lake Kasumigaura, Japan. Hydrobiologia **112**: 53–60. doi:10.1007/BF00007666

Visser, P. M., B. W. Ibelings, and L. R. Mur. 1995. Autumnal sedimentation of *Microcystis* spp. as result of an increase in carbohydrate ballast at reduced temperature. J. Plankton Res. **17**: 919–933. doi:10.1093/plankt/17.5.919

Visser, P. M., J. Passarge, and L. R. Mur. 1997. Modeling vertical migration of the cyanobacterium *Microcystis*. Hydrobiologia **349**: 99–109. doi:10.1023/A:1003001713560

Wallace, B. B., and D. P. Hamilton. 1999. The effect of variations in irradiance on buoyancy regulation in *Microcystis aeruginosa*. Limnol. Oceanogr. **44**: 273–281. doi:10.4319/lo.1999.44.2.0273

Wallace, B. B., M. C. Bailey, and D. P. Hamilton. 2000. Simulation of vertical position of buoyancy regulating *Microcystis aeruginosa* in a shallow eutrophic lake. Aquat. Sci. Res. Bound. **62**: 320–333. doi:10.1007/PL00001338

Walsby, A. 1994. Gas vesicles. Microbiol. Rev. **58**: 94–144. https://www.ncbi.nlm.nih.gov/pmc/articles/PMC372955/pdf/microrev00020-0104.pdf

Walsby, A. E., and A. Bleything. 1988. The dimensions of cyanobacterial gas vesicles in relation to their efficiency in providing buoyancy and withstanding pressure. Microbiology **134**: 2635–2645. doi:10.1099/00221287-134-10-2635

Wang, M., S. Son, Y. Zhang, and W. Shi. 2013. Remote sensing of water optical property for China's inland Lake Taihu using the SWIR atmospheric correction with 1640 and 2130 nm bands. IEEE J. Sel. Top. Appl. Earth Obs. Remote Sens. **6**: 2505–2516. doi:10.1109/JSTARS.2013.2243820

Wang, M., and C. Hu. 2016. Mapping and quantifying *Sargassum* distribution and coverage in the Central West Atlantic using MODIS observations. Remote Sens. Environ. **183**: 350–367. doi:10.1016/j.rse.2016.04.019

Wynne, T. T., R. P. Stumpf, M. C. Tomlinson, and J. Dyble. 2010. Characterizing a cyanobacterial bloom in western Lake Erie using satellite imagery and meteorological data. Limnol. Oceanogr. **55**: 2025–2036. doi:10.4319/lo.2010.55.5.2025

Xue, K., Y. Zhang, H. Duan, R. Ma, S. Loisell, and M. Zhang. 2015. A remote sensing approach to estimate vertical profile classes of phytoplankton in a eutrophic lake. Remote Sens. **7**: 14403–14427. doi:10.3390/rs71114403

Yamamoto, Y., and F.-K. Shiah. 2010. Variation in the growth of *Microcystis aeruginosa* depending on colony size and position in colonies. Ann. Limnol. Int. J. Limnol. **46**: 47–52. doi:10.1051/limn/2010006

Zhang, Y., R. Ma, M. Zhang, H. Duan, S. A. Loiselle, and J. Xu. 2015. Fourteen-year record (2000–2013) of the spatial and temporal dynamics of floating algae blooms in Lake Chaohu, observed from time series of MODIS images. Remote Sens. **7**: 10523–10542. doi:10.3390/rs70810523

Zhou, L., X. Feng, C. Wang, D. Wang, and X. Xu. 2008. Monitoring cyanobacteria bloom based on MODIS data in Lake Taihu [in Chinese]. J. Lake Sci. **20**: 203–207. doi:10.18307/2008.0211

Zohary, T., and R. D. Robarts. 1990. Hyperscums and the population dynamics of *Microcystis aeruginosa*. J. Plankton Res. **12**: 423–432. doi:10.1093/plankt/12.2.423

Acknowledgments

We thank NASA, USGS, and KORDI for providing satellite data, and also thank the two anonymous reviewers for their suggestions to improve the presentation of this paper. This work was supported by the National Key Research and Development Program of China (2016YFA0601201 and 2016YFC1400905), Key project of National Natural Science Foundation of China (41431176), China Postdoctoral Science Foundation (2017M610393) (Qi), and the U.S. NASA (NNX14AL98G).

Conflict of Interest

None declared.

Submitted 19 September 2017
Revised 24 January 2018
Accepted 14 February 2018

Associate editor: David Antoine